Environmental Science & Technology

pubs.acs.org/est

Article

Hydrodefluorination of Perfluorooctanoic Acid in the H_2-Based Membrane Catalyst-Film Reactor with Platinum Group Metal Nanoparticles: Pathways and Optimal Conditions

Min Long, Welman C. Elias, Kimberly N. Heck, Yi-Hao Luo, YenJung Sean Lai, Yan Jin, Haiwei Gu, Juan Donoso, Thomas P. Senftle, Chen Zhou,* Michael S. Wong, and Bruce E Rittmann

Cite This: *Environ. Sci. Technol.* 2021, 55, 16699−16707

Read Online

ACCESS | Metrics & More | Article Recommendations | Supporting Information

ABSTRACT: PFAAs (perfluorinated alkyl acids) have become a concern because of their widespread pollution and persistence. A previous study introduced a novel approach for removing and hydrodefluorinating perfluorooctanoic acid (PFOA) using palladium nanoparticles (Pd^0NPs) in situ synthesized on H_2-gas-transfer membranes. This work focuses on the products, pathways, and optimal catalyst conditions. Kinetic tests tracking PFOA removal, F^- release, and hydrodefluorination intermediates documented that PFOA was hydrodefluorinated by a mixture of parallel and stepwise reactions on the Pd^0NP surfaces. Slow desorption of defluorination products lowered the catalyst's activity for hydrodefluorination. Of the platinum group metals studied, Pd was overall superior to Pt, Rh, and Ru for hydrodefluorinating PFOA. pH had a strong influence on performance: PFOA was more strongly adsorbed at higher pH, but lower pH promoted defluorination. A membrane catalyst-film reactor (MCfR), containing an optimum loading of 1.2 g/m^2 Pd^0 for a total Pd amount of 22 mg, removed 3 mg/L PFOA during continuous flow for 90 days, and the removal flux was as high as 4 mg PFOA/m^2/d at a steady state. The EPA health advisory level (70 ng/L) also was achieved over the 90 days with the influent PFOA at an environmentally relevant concentration of 500 ng/L. The results document a sustainable catalytic method for the detoxification of PFOA-contaminated water.

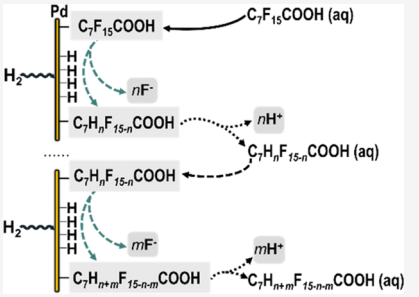

KEYWORDS: *perfluorooctanoic acid (PFOA), palladium, nanoparticle, hydrodefluorination*

INTRODUCTION

PFAAs (perfluorinated alkyl acids) are attracting global attention as emerging contaminants because of their persistence and bioaccumulation.[1] PFAAs are man-made chemicals that have widespread use in paper coatings, fabrics, polymers, adhesives, and firefighting foams.[2] PFOA (perfluorooctanoic acid), one of the most widely used PFAAs, is a common contaminant in soil and groundwater globally,[2,3] and its accumulation in humans and other organisms leads to adverse health impacts.[4] Therefore, the USEPA has recommended a health advisory level for PFOA and PFOS (perfluorooctanesulfonic acid) in the drinking water of 70 ng/L.[5]

Due to its very strong carbon−fluorine bond (440.99 kJ/mole), PFOA resists chemical, thermal, and biological breakdown under ambient conditions.[6] Effective destructive approaches—based on sonochemical, thermal, chemical oxidation, and chemical reduction—require large energy inputs.[3,7] Nondestructive removal methods, such as adsorption by GAC, ion exchange, nanofiltration, and reverse osmosis, only separate PFOA, which produces residues that require further treatment or disposal.[6]

Precious-metal catalysts, including gold, silver, and the six platinum group metals (PGMs) (ruthenium (Ru), rhodium (Rh), palladium (Pd), osmium (Os), iridium (Ir), and platinum (Pt)), are promising for treating halogenated contaminants,[8] because they can have high dehalogenation activity and resist being oxidized or corroded.[9] In particular, precious-metal catalysts have been reported to hydrodefluorinate compounds such as polyfluorinated arenes[10] and fluorinated pharmaceuticals.[11] The most common and sustainable electron donor used for catalytic reductions is H_2 gas, as long as it can be supplied in a controllable and efficient way.[12]

A H_2-based membrane catalyst-film reactor (H_2-MCfR) is a novel technology that can overcome the challenges of low efficiency and safety of H_2 delivery by accurately supplying H_2 gas in a bubble-free form through nonporous membrane fibers. This efficient and accurate way in delivering H_2 enables the formation of a robust catalyst film, high-efficiency utilization of H_2, and minimal combustion potential.[13,14]

Received: September 27, 2021
Revised: November 24, 2021
Accepted: November 29, 2021
Published: December 7, 2021

We recently reported that palladium nanoparticles (Pd^0NPs) were able to catalyze hydrodefluorination of PFOA under ambient conditions in a H_2-MCfR platform.[15] We also proposed two distinct adsorption modes of PFOA on Pd^0NP surfaces, which are responsible for driving PFOA removal. Here, we identified pathways of Pd^0-catalytic hydrodefluorination of PFOA by tracking the production of intermediates. We also investigated optimal catalytic conditions, including catalyst types (Pd versus Pt, Rh, and Ru), catalyst loading, and pH. Finally, we document ~90 days of continuous operations with a range of surface loadings of PFOA.

MATERIALS AND METHODS

MCfR Setup. The reactor setup, shown in Figure S1, was similar to the one used in our previous study.[15,16] The reactor was made of glass and contained one bundle of 120 membrane fibers (polypropylene; Teijin, Ltd., Japan) having an outer diameter of 200 μm, an inner diameter of 100 μm, and a wall thickness of 50 μm. The total surface area of the membrane fibers was 184 cm^2, and the working volume was 40 mL. The reactor had an internal diameter of 6 mm, and the length of the glass tube was 27 cm. One recirculating pump was used to mix the liquid thoroughly at a rate of 150 mL/min (at least 1500 times of the influent rate) (Masterflex, USA). Hydrogen gas (H_2) was supplied to both ends of the bundle from a gas cylinder and a pressure regulator.

Synthesis and Deposition of Catalysts. We chose four types of PGMs (Pt, Pd, Rh, and Ru) that are known hydrogenation catalysts. We prepared the PGM precursor solutions by dissolving each of the PGM salts—sodium tetrachloropalladate (Na_2PdCl_4), sodium tetrachloroplatinate (Na_2PtCl_4), potassium hexachlororhodate (K_3RhCl_6), or potassium pentachlororuthenate (K_2RuCl_5)—into deionized (DI) water and adjusting the solution pH to 6.5 by addition of 10 mM phosphate buffer. For each batch or continuous test, we used freshly prepared catalysts. The MCfR was fed with the PGM precursor solution and then kept in batch mode for 24 h until more than 99% of the PGM cation was reduced to its elemental form and deposited on the membrane surface; the MCfRs were then drained, rinsed with DI water three times, and then fed with PFOA stock solution for the test.

Solid-State Characterization. Fiber pieces were cut from an MCfR fiber, and samples were prepared following our established protocol.[16] X-ray powder diffraction analysis was conducted using Philips X'Pert Pro equipment with a Cu Kα radiation source (1.5406 Å) from 10 to 90 2θ degrees range with a step size of 0.0050 s^{-1}. We used an FEI Titan environmental transmission electron microscope (ETEM) to characterize the catalysts by imaging and crystallite diffraction. We carried out X-ray photoelectron spectroscopy using a PHI Quantera SXM (ULVAC-PHI. Inc) with an Al source (focused beam of 1.5 kV, 25 W).

Batch Tests. We conducted a series of batch tests as a means to find the optimal conditions on the deposited elemental Pd^0NPs for defluorination of PFOA. Each batch test was conducted in triplicate. To begin each batch operation, the MCfR was purged with pure N_2 gas for at least 15 min, and then, the PFOA stock solution was rapidly introduced into the MCfR using a feeding pump.

For the initial batch test, after the deposition of 1.2 g Pd^0/m^2 on the membrane fibers, we evaluated the defluorination process by feeding the reactor with 10 μM PFOA with the conditions of 20 psi H_2, pH 4, and a duration of 60 h. At the end of the experiment, we removed the Pd fibers from the membrane, rinsed them with DI water three times, and dissolved the catalyst in 1 M hydrochloric acid overnight. We adjusted the pH of the Pd dissolution liquid to ~3 and then used high-performance liquid chromatography−quadrupole time-of-flight mass spectrometry (HPLC-QTOF-MS) to analyze for compounds in the liquid.

For the experiments evaluating the different catalysts, we evaluated Pt, Pd, Rh, or Ru for the conditions of ~10 μM PFOA, 20 psi H_2, and pH 4. For the Pd^0-loading tests, we tested different loadings of Pd^0 (0.2, 0.7, 1.2, 2.3, and 4.5 g/m^2) for removing and defluorinating PFOA with the conditions of ~10 μM PFOA, 20 psig H_2, and at pH 4. For the pH tests, we conducted defluorination tests at pH 4, 5, 6, or 7 using a Pd^0NP loading of 1.2 g Pd^0/m^2, 20 psig H_2, and ~10 μM PFOA. We adjusted the pH by using phosphate buffer.

Continuous Tests. We set up three freshly produced H_2-MCfRs, each having 1.2 g Pd^0/m^2, for continuous removal of PFOA fed at different surface loadings obtained by adjusting the influent concentration and hydraulic retention time (HRT). MCfR #A had 6 ppm PFOA in the influent and an HRT at 6 h, giving a PFOA surface loading of 48 mg/m^2/d. MCfR #B had 3 ppm PFOA in the influent, an HRT at 24 h, and a PFOA surface loading at 5.8 mg/m^2/d. MCfR #C had a more environmentally relevant influent concentration of ~500 ppt PFOA, an HRT of 24 h, and a PFOA surface loading at 0.8 μg/m^2/d.

Sampling and Analyses. We took effluent samples from the MCfRs using 3 mL syringes and then filtered them immediately through 0.2 μm membrane filters. We measured PFOA (>0.1 μM) and F^- (>0.5 μM) using an ion chromatograph (IC-930, Metrohm, USA) equipped with a C18 column (a calibration curve is given in Section 5 in the Supporting Information). We also used an Oakton Ion 700 fluoride electrode and Hach TNT 878 kits to verify the F^- results detected by IC; Section 5 in the Supporting Information provides the details. The differences of the observed concentration values for the same sample were consistently <10%. We detected intermediates of PFOA through HPLC-QTOF-MS. We determined PFOA at the ppt level using an Agilent 6490 UPLC coupled to a triple quadrupole mass spectrometer system (QQQ-MS). Details of these analytical methods are given in Section 1 of the Supporting Information.

Calculations. The defluorination ratio was calculated from:

$$\text{defluorination ratio} = \frac{C_F}{15(C_0 - C_{PFOA})} \quad (1)$$

where C_F refers to the fluoride concentration (μM) measured at the reactor exit, C_0 refers to the initial PFOA concentration, and C_{PFOA} refers to the PFOA concentration (μM) measured at the reactor exit.

The PFOA surface loading (J_{SL}) (in the units of g/m^2/day) was calculated with:

$$J_{SL} = C_0\frac{Q}{A} \quad (2)$$

and the PFOA-removal flux (J_{flux}) (in the units of g/m^2/day) was calculated with:

$$J_{flux} = (C_0 - C_{PFOA})\frac{Q}{A} \quad (3)$$

https://doi.org/10.1021/acs.est.1c06528
Environ. Sci. Technol. 2021, 55, 16699−16707

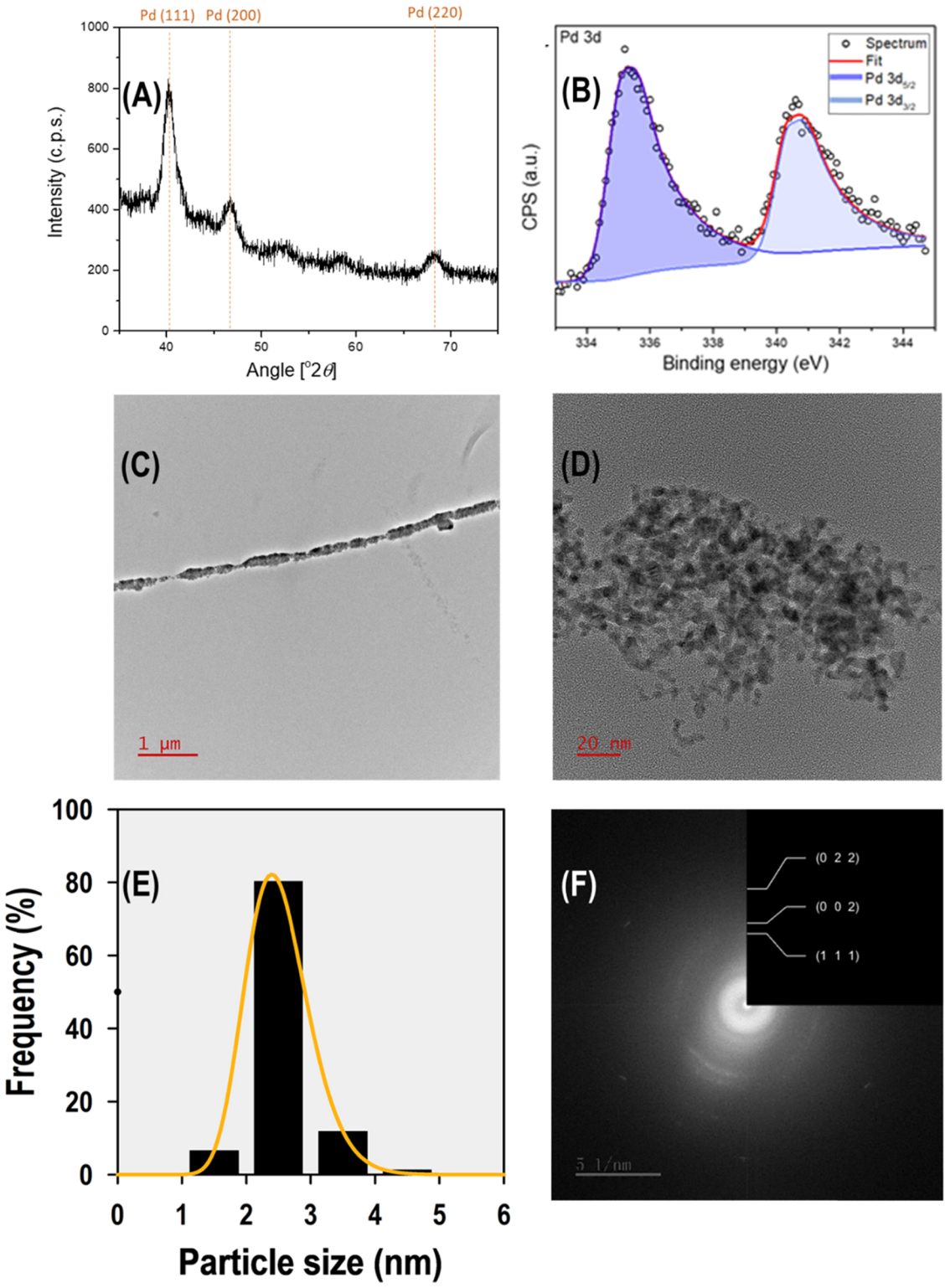

Figure 1. (A) XRD spectra of a Pd fiber. (B) XPS spectra of a Pd fiber. (C) TEM image of the cross section of a Pd fiber. (D) TEM image of a Pd fiber. (E) Size distribution of the nanoparticles of figure D. (F) Diffraction patterns of Pd^0NPs from figure D.

where Q refers to the flow rate (L/day), and A refers to the total fiber surface area (18.48×10^{-3} m^2).[20]

RESULTS AND DISCUSSION

Characteristics of the Pd Film in the MCfR. Figure 1 displays characteristics of a Pd film in the MCfR with a Pd^0 loading of 1.2 g Pd^0/m^2. XPS analysis of the Pd fiber (Figure 1B) showed only the presence of one peak at $Pd_{3/2}$ and $Pd_{5/2}$ energy, centered at 340.7 and 335.4 eV, which is attributed to Pd^0.[17,18] The XRD pattern in Figure 1A verifies the presence of crystalline Pd, with its three characteristic diffraction peaks at 40.3, 46.7, and 68.2 2θ degrees assigned to the (111), (200), and (220) planes, respectively. The calculated crystallite size on the basis of the Scherrer equation is 6.0 nm. TEM images of

https://doi.org/10.1021/acs.est.1c06528
Environ. Sci. Technol. 2021, 55, 16699−16707

the cross section of the Pd film (Figure 1C,D) show that Pd^0NPs were attached onto the membrane fibers, forming a NP-containing layer with a thickness of ~60 nm. The Pd^0NP's size (Figure 1E) was 2.6 ± 0.5 nm (based on 152 particles in Figure 1D), which is similar to previous MCfR studies.[16,19] The diffraction patterns (Figure 1F) show three planes of Pd^0: (111), (200), and (220), the same planes observed by XRD.

PFOA Hydrodefluorination on the Pd^0NP Surface. *Mixed Parallel and Stepwise Hydrodefluorination of PFOA to Partially or Nonfluorinated OAs.* In the batch experiment with 1.2 g Pd^0/m^2 on the membrane fibers, presented in Figure 2A, over 99% of the initial 10 μM PFOA was depleted within

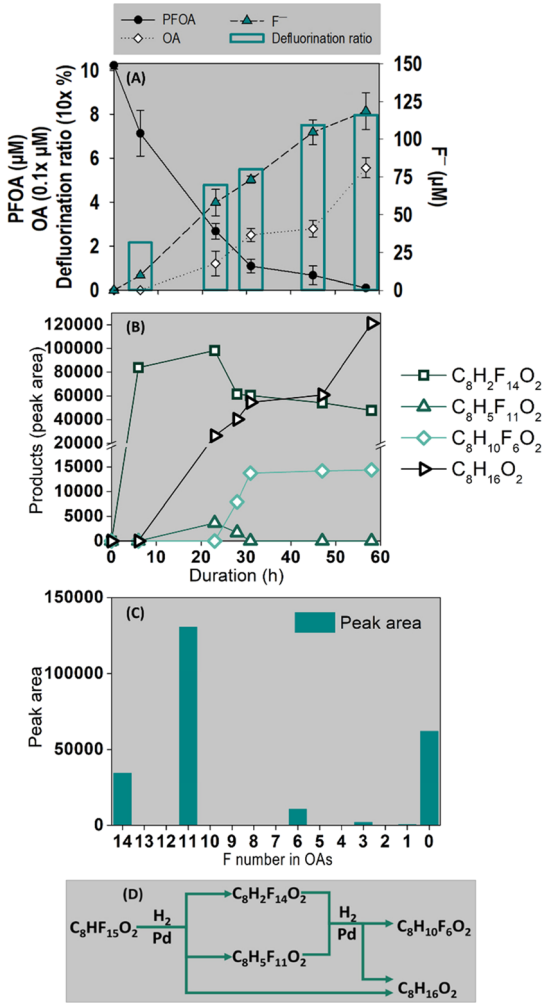

Figure 2. (A) Average concentrations ± standard deviations of PFOA and F^- released in the batch tests of catalytic reductive defluorination of ~10 μM PFOA in the MCfR with 5 mM Pd^0NPs at pH ~4 with H_2 of 20 psig. (B) Products detected in the bulk liquid. (C) Compounds adsorbed on the Pd surface. (D) Example of mixed parallel and stepwise defluorination.

58 h, which was accompanied by steady F^- release up to 0.12 mM (77.3% of the F originally present on the depleted PFOA) at the end of the experiment. In supplementary tests (Section 3 in the Supporting Information), using Pd/Al_2O_3 powder at the same 500:1 mole ratio of Pd to PFOA, no defluorination occurred in the presence of headspace H_2. Thus, H_2 directly transferred to Pd^0 deposited in situ on the membranes was what enabled the defluorination of PFOA in the MCfR. CO adsorption tests (Section 4 in the Supporting Information) further indicated that only a small amount of Pd on the membrane was exposed, but it was extraordinarily active for the hydrodefluorination reaction. The HPLC-QTOF-MS results in Figure 2B reveal the presence of three partially hydrodefluorinated fluorooctanoic acids (FOAs)—$C_8H_2F_{14}O_2$, $C_8H_5F_{11}O_2$, and $C_8H_{10}F_6O_2$—along with 5.4% selectivity to completely hydrodefluorinated OA ($C_8H_{16}O_2$) in the bulk liquid during the batch experiment. We detected no alcohol products, which supports the understanding that Pd^0 cannot reduce the carboxylate group into alcohol.[1] Thus, the products confirmed that Pd^0-catalytic PFOA conversion was exclusively via reductive hydrodefluorination:

$$C_7F_{15}COOH + nH_2 \rightarrow C_7H_nF_{15-n}COOH + nH^+ + nF^- \quad (1 \le n \le 15) \tag{4}$$

The defluorination ratio (eq 1) increased from 20% in the first 6 h to 77% at 58 h, which supports that PFOA was sequentially hydrodefluorinated after being removed from water. Among the defluorination products (Figure 2B), lightly defluorinated $C_8H_2F_{14}O_2$ and $C_8H_5F_{11}O_2$ accumulated during the first 6−23 h but then were depleted. More completely defluorinated products, such as $C_8H_{10}F_6O_2$ and $C_8H_{16}O_2$, appeared once $C_8H_2F_{14}O_2$ and $C_8H_5F_{11}O_2$ began to decline. These trends further support the occurrence of stepwise hydrodefluorination. Because the lightly defluorinated species appeared and then declined in solution, they desorbed and then resorbed onto the Pd^0NP surfaces for further defluorination:

$$C_7H_nF_{15-n}COOH + mH_2 \rightarrow C_7H_{n+m}F_{15-n-m}COOH + mH^+ + mF^- \quad (1 \le m \le n) \tag{5}$$

This phenomenon is similar to Pd^0-catalyzed hydrodehalogenation of chlorophenol to phenol, with subsequent hydrogenation to cyclohexanone.[20]

Defluorination Products of PFOA Were Retained on Pd^0NP Surfaces. Figure 2C shows OA and three partially defluorinated OAs in the digested solution of the Pd film after the 58 h batch test. All four species also were found in the bulk liquid during the batch test (Figure 2B). This indicates that defluorination products were retained on the Pd^0 surface, which infers that desorption was slower than defluorination. Slow desorption of the FOAs contrasts to Pd^0-catalyzed dehalogenation of trichloroacetic acid in which desorption was not a rate-limiting step.[13] This difference probably was caused by higher adsorption affinity of longer-chain fatty acids from PFOA.[21]

The persistence of surface-bound FOA complexes may affect the catalyst's activity. Figure 3 presents results from a set of batch experiments with higher initial concentrations of PFOA in different MCfRs. Initial first-order rates of PFOA removal and defluorination were considerably lower as the PFOA concentration increased from 10 to 1000 μM. In particular, PFOA removal halted after 40 h and defluorination was minimal when the initial PFOA concentration was 1000 μM. FTIR spectra of the Pd films in the three MCfRs at the end of the experiments reveal the symmetric (1450 cm^{-1}) and asymmetric (1650 cm^{-1}) stretching of the COO^- group[22−24] for 100 μM PFOA, and the signals were higher for 1000 μM PFOA. This supports that retained Pd-FOA complexes

https://doi.org/10.1021/acs.est.1c06528
Environ. Sci. Technol. 2021, 55, 16699−16707

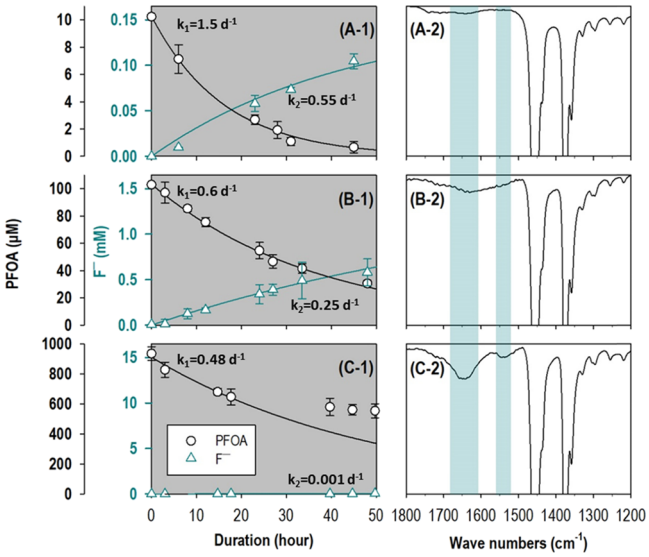

Figure 3. (Left panels) Average concentrations ± standard deviations of PFOA and F^- released in the batch test with an influent concentration of 10, 100, or 1000 μM PFOA catalyzed by 1.2 g Pd^0/m^2 at pH 4 in the MCfR. (Right panels) Corresponding FTIR spectrum of the Pd surface after the reactions. First-order rate coefficients for PFOA loss (k_1) and F^- release (k_2) are in units of d^{-1}.

retarded PFOA hydrodefluorination by blocking active sites on the Pd^0 surface.

Proposed Pathway of PFOA Hydrodefluorination. Based on the products detected from the liquid and the Pd^0 surface, we propose in Figure 4 a pathway of PFOA hydro-

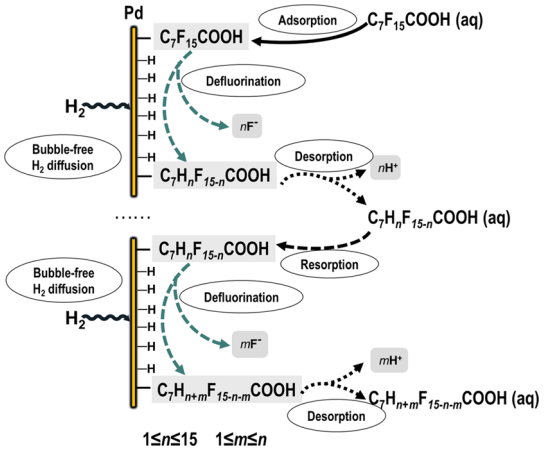

Figure 4. Proposed pathway of PFOA hydrodefluorination by Pd^0NPs in the MCfR.

defluorination catalyzed by Pd^0NPs in the presence of H_2. After H_2 diffused through the nonporous membrane and reached the Pd^0 surface, it dissociated into the single activated H atoms adsorbed on the Pd^0 surfaces (i.e., H^*_{ads}) on the bulk liquid side.[13] PFOA in the bulk liquid adsorbed on Pd^0 surfaces, forming Pd-PFOA complexes. Abundant H^*_{ads} on the surface enabled the reductive release of F^-,[13,15] transforming $C_7F_{15}COOH^*$ (i.e., Pd-PFOA) to various forms, such as $C_7H_nF_{15-n}COOH^*$ or Pd-$C_7H_nF_{15-n}COOH$ (e.g., $C_7HF_{14}COOH$ observed in this study) in parallel:

$$\boxed{Pd} - C_7F_{15}COOH^* + n\boxed{Pd} - H^*_{ads} \rightarrow \boxed{Pd} - C_7H_nF_{15-n}COOH^* + nF^- \ (1 \le n \le 15) \quad (6)$$

These partially defluorinated complexes could be further hydrogenated and then desorbed into the bulk liquid as the free $C_7H_nF_{15-n}COOH$ form:

$$\boxed{Pd} - C_7H_nF_{15-n}COOH^* + n\boxed{Pd} - H^*_{ads} \rightarrow C_7H_nF_{15-n}COOH + nH^+ \ (1 \le n \le 15) \quad (7)$$

We postulate that desorption became the rate-limiting step of the entire defluorination process, and it also led to the accumulation of some partially defluorinated products on the Pd^0NP active sites.

Some of the released products probably were resorbed by Pd^0NPs, formed $C_7H_nF_{15-n}COOH^*$, and were hydrodefluorinated into $C_7H_{n+m}F_{15-n-m}COOH^*$:

$$\boxed{Pd} - C_7H_nF_{15-n}COOH^* + m\boxed{Pd} - H^*_{ads} \rightarrow \boxed{Pd} - C_7H_{n+m}F_{15-n-m}COOH^* + mF^- \ (1 \le m \le n) \quad (8)$$

Further hydrogeneration and desorption steps were possible, e.g.,

$$\boxed{Pd} - C_7H_{n+m}F_{15-n-m}COOH^* + m\boxed{Pd} - H^*_{ads} \rightarrow C_7H_{n+m}F_{15-n-m}COOH + mH^+ \ (1 \le m \le n) \quad (9)$$

Optimal Conditions for Catalytic Defluorination. Figure 5 summarizes the results for the removal and defluorination of 10 μM PFOA for various conditions in the MCfR, with the default condition at 20 psig (2.38 atm absolute) H_2 pressure and room temperature (22 °C). Figures S2−S4 provide more detailed information.

Pd^0 Was Overall Superior to the Other Three PGMs. Figures 5A and S2 show the concentration changes of PFOA and F^- over time in batch experiments with four PGM catalysts with the same loading of 5 mM M (Pd, Pt, Ru, and Rh) and at pH 4. Pt, Ru, and Rh exhibited moderately higher PFOA-removal rates than Pd^0, but Pd^0 had at least 15-fold faster defluorination kinetics (maximal 2.52 mM/h) and capacity (77% within 50 h) than the other three PGM catalysts. The unique catalytic activity of Pd^0 probably was caused by its superior capacity for H_2 adsorption at acidic pH.[9,25] Moreover, we hypothesize that with H_2 being delivered efficiently Pd^0 was able to form a stable bulk hydride, since hydrogen can readily "dissolve" in the Pd lattice.[26,27] This suggests that the hydrogen-rich "beta-phase" of PdH was the catalyst's active phase, responsible for defluorination. Rh, Pt, and Ru displayed limited defluorination capability at acidic pH, a finding similar to treating fluorinated pharmaceuticals.[11] Overall, Pd^0 was superior to the other PGMs in defluorinating PFOA at pH 4.

Effects of Pd^0 Loading. Figures 5B and S3 show the time-dependent concentration profiles for the different Pd^0 loadings at pH 4. With more Pd^0 coated onto the membranes of the H_2-MCfRs (from 0.2 to 4.5 g/m^2 Pd), catalytic activities for PFOA removal monotonically decreased, but the defluorination rate constant (maximal 1.04 L/g Pd^0/d) and capacity (77%) reached peaks at 1.2 g/m^2. When the Pd^0 loading exceeded 1.2 g Pd^0/m^2, the catalytic defluorination rate decreased sharply, by ~350-fold. This peaking at 1.2 g Pd^0/m^2 occurred because the defluorination of PFOA with H_2 occurred mainly at the

https://doi.org/10.1021/acs.est.1c06528
Environ. Sci. Technol. 2021, 55, 16699−16707

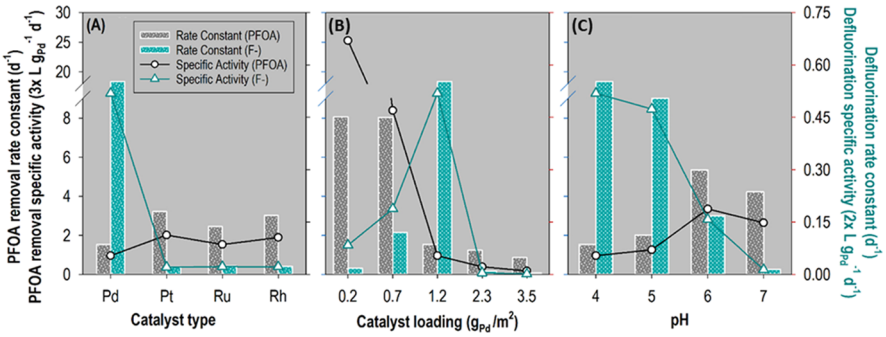

Figure 5. PFOA removal and defluorination kinetics estimated from the average experimental results for various conditions in the batch MCfRs. The default condition was 10 μM initial PFOA, 20 psig (2.36 atm absolute) H_2 pressure, and room temperature (22 °C).

water−Pd^0 interface. We hypothesize that while increasing the loading of nanoparticles increased the total active surface area,[28] excessive Pd^0 coverage resulted in aggregation of Pd^0NPs, which decreased the accessible specific surface area and led to lower catalytic activity.[14] In addition, a thick and agglomerated Pd film may have hindered H_2 transfer to Pd^0 sites near the bulk liquid. Because 1.2 g Pd^0/m^2 gave the best removal and defluorination performance, it was chosen as the optimal addition in this study.

PFOA Was More Strongly Adsorbed at Higher pH, but Lower pH Promoted Defluorination. Figures 5C and S4 further compare how pH affected Pd^0 catalytic reduction of PFOA with the same Pd^0 loading of 1.2 g/m^2 and a constant H_2 pressure of 20 psig. At pH 4, over 99% of the 10 μM PFOA was depleted, along with the accumulation of 0.118 mM F^- (accounting for 77% of the total F in the 10 μM PFOA) within 47 h. When the pH was raised from 4 to 7, the removal rate of PFOA increased gradually, and the PFOA-removal rate was ~threefold faster than that at pH 4. However, the defluorination rate decreased monotonically, becoming ~38-fold slower at pH 7 than that at pH 4. Pd^0 has higher capacity for H_2 adsorption at acidic pH,[9,25] which should promote defluorination at lower pH.[29,30] Also, the Pd^0 surface is more negatively charged with increasing pH, which will generate stronger electrostatic repulsion between $PFOA^-$ and the Pd^0 surface, resulting in less defluorination.[31−33] Other anions (e.g., OH^- and CO_3^{2-}) also are more subject to being adsorbed on the Pd^0 surface at higher pH, and this competes with $PFOA^-$ for active catalytic sites.[9,29,34] In summary, PFOA was more strongly adsorbed at higher pH, but lower pH promoted defluorination.

Summary: 1.2 g/m^2 Pd Catalysts at pH 4 Have Achieved the Best Defluorination Efficiency of PFOA. Based on all the PFOA removal and defluorination results in Figure 5, 1.2 g/m^2 Pd^0 at pH 4 achieved the best PFOA defluorination efficiency, with a maximum defluorination rate of 2.5 μM/h and a defluorination first-order rate constant of 0.55 day^{-1}.

Continuous Tests on Varied Loadings of PFOA. Figure 6 displays results for three MCfRs continuously fed in parallel with a range of surface loadings of PFOA; all had 1.2 g Pd^0/m^2 and a constant H_2 pressure of 20 psig (2.38 atm absolute) at pH 6.

MCfR-A tested a high influent PFOA concentration (6 mg/L or 14 μM) and a short HRT (6 h); results are shown in Figure 6A. The resulting PFOA surface loading was 48 mg/m^2/d or 0.12 mmol/m^2/d, and the average concentration of effluent PFOA was 6.9 μM (49% removal) for the first 15 days. Then, the PFOA concentration increased quickly and exceeded

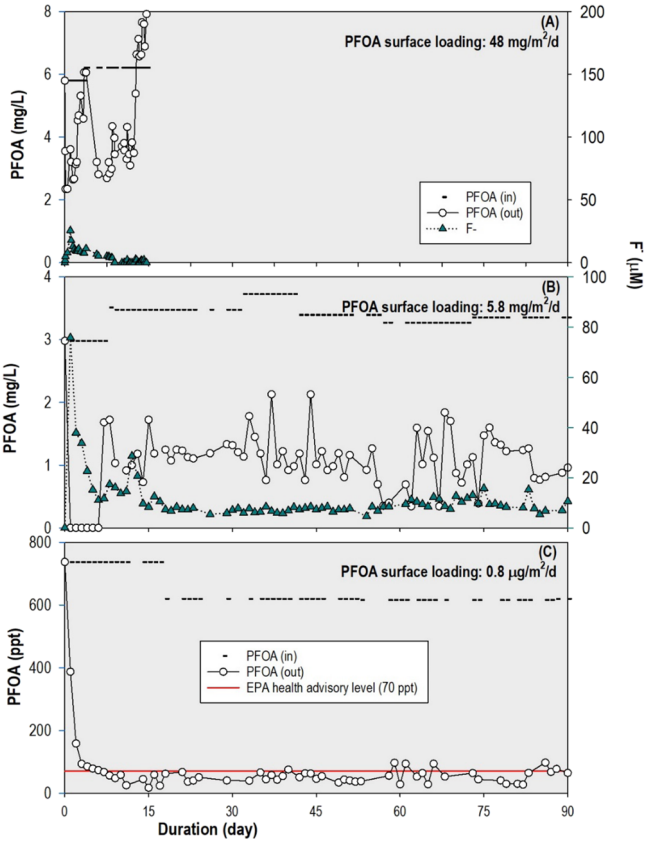

Figure 6. Concentrations of PFOA and F^- in the effluents of three continuously operated MCfRs loaded with identical 1.2 g Pd^0/m^2 and supplied with PFOA with surface loading at 48 mg/m^2/d, 5.8 mg/m^2/d, or 0.8 μg/m^2/d (top to bottom).

the influent PFOA concentration by 27%. The F^- concentration was 0.025 mM with a defluorination ratio of 12% within the first 3 days but then F^- decreased gradually to 0.002 mM (defluorination ratio ~1%) out to day 15. The results in Figure 6A verify that a high PFOA surface loading saturated and deactivated the Pd^0NPs.

MCfR-B had a lower PFOA surface loading, 5.8 mg/m^2/d (0.014 mmol/m^2/d), achieved by halving the influent concentration and extending HRT to 24 h; its results are shown in Figure 6B. The removal of PFOA stabilized at 67.9 ± 11.2% for about 90 days, and the highest removal flux was 4 mg/m^2/d (or 0.01 mmol/m^2/d). Correspondingly, the effluent F^- stabilized at 8.5 ± 2.2 μM, which was 10.5 ± 2.7% of the F in the depleted PFOA.

https://doi.org/10.1021/acs.est.1c06528
Environ. Sci. Technol. 2021, 55, 16699−16707

MCfR-C (Figure 6C) tested a more environmentally relevant PFOA concentration of 500 ng/L (1.2 nM).[35,36] The PFOA surface loading was 0.8 $\mu g/m^2/d$ (1.9 $nmol/m^2/d$). Within 4 days, the effluent PFOA decreased to <100 ng/L (0.24 nM, or 87% removal). After day 4, the effluent concentration of PFOA was consistently below the EPA health advisory level (70 ng/L or 0.17 nM), with an average concentration of 57.1 ± 24.7 ng/L or 0.14 ± 0.06 nM (88.1 ± 5.4% removal), for the following 86 days. During continuous operation, total Pd loss during 90 days was only 4.6% of the total Pd deposited on the membrane (Figure S5), which is minimal compared to previous studies with immobilized Pd.[37,38] After being exposed to PFOA, the crystallinity of Pd^0 did not change (Figure S6).

Overall, continuous operation documented long-term PFOA removal and reductive defluorination when the PFOA surface loading was ≤5.8 $mg/m^2/d$. The EPA health advisory level of ≤70 ng/L could be attained with a surface loading of ≤0.8 $\mu g/m^2/d$. Much higher PFOA surface loading led to saturation and deactivation of Pd^0NPs.

■ ASSOCIATED CONTENT

Supporting Information

The Supporting Information is available free of charge at https://pubs.acs.org/doi/10.1021/acs.est.1c06528.

Chromatographic methods; schematic of the bench-scale MCfR system; removal and defluorination of 10 μM PFOA catalyzed by various PGMs; removal and defluorination of 10 μM PFOA catalyzed by Pd^0 with varied loadings; removal and defluorination of 10 μM PFOA catalyzed by Pd at varied pH levels; total Pd in the effluent and Pd loss conditions for 90 days; XRD result of post catalysis; supplementary test on Pd/Al_2O_3 powder; CO chemisorption tests; and F^- verification by IC, the fluoride electrode, and colorimetry (PDF)

■ AUTHOR INFORMATION

Corresponding Author

Chen Zhou − *Biodesign Swette Center for Environmental Biotechnology, Arizona State University, Tempe, Arizona 85287-5701, United States; Nanosystems Engineering Research Center for Nanotechnology Enabled Water Treatment, Houston, Texas 77005, United States;* orcid.org/0000-0002-8104-2848; Email: zhou_SCEB@asu.edu

Authors

Min Long − *Biodesign Swette Center for Environmental Biotechnology, Arizona State University, Tempe, Arizona 85287-5701, United States; Nanosystems Engineering Research Center for Nanotechnology Enabled Water Treatment, Houston, Texas 77005, United States;* orcid.org/0000-0001-5328-7787

Welman C. Elias − *Department of Chemical and Biomolecular Engineering, Rice University, Houston, Texas 77005-1892, United States*

Kimberly N. Heck − *Nanosystems Engineering Research Center for Nanotechnology Enabled Water Treatment, Houston, Texas 77005, United States; Department of Chemical and Biomolecular Engineering, Rice University, Houston, Texas 77005-1892, United States*

Yi-Hao Luo − *Biodesign Swette Center for Environmental Biotechnology, Arizona State University, Tempe, Arizona 85287-5701, United States;* orcid.org/0000-0001-8975-8579

YenJung Sean Lai − *Biodesign Swette Center for Environmental Biotechnology, Arizona State University, Tempe, Arizona 85287-5701, United States*

Yan Jin − *Arizona Metabolomics Laboratory, College of Health Solutions, Arizona State University, Phoenix, Arizona 85004, United States*

Haiwei Gu − *Arizona Metabolomics Laboratory, College of Health Solutions, Arizona State University, Phoenix, Arizona 85004, United States;* orcid.org/0000-0002-7598-5022

Juan Donoso − *Nanosystems Engineering Research Center for Nanotechnology Enabled Water Treatment, Houston, Texas 77005, United States; Department of Chemical and Biomolecular Engineering, Rice University, Houston, Texas 77005-1892, United States*

Thomas P. Senftle − *Nanosystems Engineering Research Center for Nanotechnology Enabled Water Treatment, Houston, Texas 77005, United States; Department of Chemical and Biomolecular Engineering, Rice University, Houston, Texas 77005-1892, United States;* orcid.org/0000-0002-5889-5009

Michael S. Wong − *Nanosystems Engineering Research Center for Nanotechnology Enabled Water Treatment, Houston, Texas 77005, United States; Department of Chemical and Biomolecular Engineering, Rice University, Houston, Texas 77005-1892, United States;* orcid.org/0000-0002-3652-3378

Bruce E Rittmann − *Biodesign Swette Center for Environmental Biotechnology, Arizona State University, Tempe, Arizona 85287-5701, United States; Nanosystems Engineering Research Center for Nanotechnology Enabled Water Treatment, Houston, Texas 77005, United States*

Complete contact information is available at: https://pubs.acs.org/10.1021/acs.est.1c06528

Notes

The authors declare no competing financial interest.

■ ACKNOWLEDGMENTS

This work was partially supported by the National Science Foundation Engineering Research Center for Nanotechnology Enabled Water Treatment (EEC-1449500), the Strategic Environmental Research and Development Program (SERDP) (ER20-C1-1286), and Xylem Inc. (FP00019503). We acknowledge the use of facilities within the Eyring Materials Center and Mass Spectrometry at Arizona State University and the staff scientist involved in the data collection.

■ REFERENCES

(1) Lee, Y.-C.; Chen, Y.-P.; Chen, M.-J.; Kuo, J.; Lo, S.-L. Reductive defluorination of perfluorooctanoic acid by titanium (III) citrate with vitamin B12 and copper nanoparticles. *J. Hazard. Mater.* **2017**, *340*, 336−343.

(2) Moody, C. A.; Field, J. A. Perfluorinated surfactants and the environmental implications of their use in fire-fighting foams. *Environ. Sci. Technol.* **2000**, *34*, 3864−3870.

(3) Mahinroosta, R.; Senevirathna, L. A review of the emerging treatment technologies for PFAS contaminated soils. *J. Environ. Manage.* **2020**, *255*, No. 109896.

(4) Olsen, G. W.; Mair, D. C.; Lange, C. C.; Harrington, L. M.; Church, T. R.; Goldberg, C. L.; Herron, R. M.; Hanna, H.; Nobiletti, J. B.; Rios, J. A.; Reagen, W. K.; Ley, C. A. Per-and polyfluoroalkyl substances (PFAS) in American Red Cross adult blood donors, 2000−2015. *Environ. Res.* **2017**, *157*, 87−95.
(5) USEPA, Fact sheet: PFOA & PFOS drinking water health advisories (accessed April, 2018). https://www.epa.gov/ground-water-and-drinking-water/drinking-water-health-advisories-pfoa-and-pfos, 2016.
(6) Huang, S.; Jaffé, P. R. Defluorination of perfluorooctanoic acid (PFOA) and perfluorooctane sulfonate (PFOS) by Acidimicrobium sp. strain A6. *Environ. Sci. Technol.* **2019**, *53*, 11410−11419.
(7) Merino, N.; Qu, Y.; Deeb, R. A.; Hawley, E. L.; Hoffmann, M. R.; Mahendra, S. Degradation and removal methods for perfluoroalkyl and polyfluoroalkyl substances in water. *Environ. Eng. Sci.* **2016**, *33*, 615−649.
(8) Rylander, P., *Catalytic hydrogenation over platinum metals*; Elsevier: 2012.
(9) Clark, C. A.; Reddy, C. P.; Xu, H.; Heck, K. N.; Luo, G.; Senftle, T. P.; Wong, M. S. Mechanistic Insights into pH-controlled nitrite reduction to ammonia and hydrazine over rhodium. *ACS Catal.* **2019**, *10*, 494−509.
(10) Baumgartner, R.; Stieger, G. K.; McNeill, K. Complete hydrodehalogenation of polyfluorinated and other polyhalogenated benzenes under mild catalytic conditions. *Environ. Sci. Technol.* **2013**, *47*, 6545−6553.
(11) Park, J.; An, S.; Jho, E. H.; Bae, S.; Choi, Y.; Choe, J. K. Exploring reductive degradation of fluorinated pharmaceuticals using Al2O3-supported Pt-group metallic catalysts: Catalytic reactivity, reaction pathways, and toxicity assessment. *Water Res.* **2020**, *185*, No. 116242.
(12) Long, M.; Ilhan, Z. E.; Xia, S.; Zhou, C.; Rittmann, B. E. Complete dechlorination and mineralization of pentachlorophenol (PCP) in a hydrogen-based membrane biofilm reactor (MBfR). *Water Res.* **2018**, *144*, 134−144.
(13) Luo, Y.-H.; Zhou, C.; Bi, Y.; Long, X.; Wang, B.; Tang, Y.; Krajmalnik-Brown, R.; Rittmann, B. E. Long-Term Continuous Co-reduction of 1, 1, 1-Trichloroethane and Trichloroethene over Palladium Nanoparticles Spontaneously Deposited on H2-Transfer Membranes. *Environ. Sci. Technol.* **2021**, *55*, 2057.
(14) Zhou, D.; Luo, Y.-H.; Zheng, C.-W.; Long, M.; Long, X.; Bi, Y.; Zheng, X.; Zhou, C.; Rittmann, B. E. H2-Based Membrane Catalyst-Film Reactor (H2-MCfR) Loaded with Palladium for Removing Oxidized Contaminants in Water. *Environ. Sci. Technol.* **2021**, *55*, 7082−7093.
(15) Long, M.; Donoso, J.; Bhati, M.; Elias, W. C.; Heck, K. N.; Luo, Y.-H.; Lai, Y. S.; Gu, H.; Senftle, T. P.; Zhou, C.; Wong, M. S.; Rittmann, B. E. Adsorption and Reductive Defluorination of Perfluorooctanoic Acid over Palladium Nanoparticles. *Environ. Sci. Technol.* **2021**, *55*, 14836.
(16) Zhou, C.; Wang, Z.; Ontiveros-Valencia, A.; Long, M.; Lai, C.-Y.; Zhao, H.-P.; Xia, S.; Rittmann, B. E. Coupling of Pd nanoparticles and denitrifying biofilm promotes H_2-based nitrate removal with greater selectivity towards N_2. *Appl. Catal., B* **2017**, *206*, 461−470.
(17) Elias, W. C.; Signori, A. M.; Zaramello, L.; Albuquerque, B. L.; de Oliveira, D. C.; Domingos, J. B. Mechanism of a Suzuki-type homocoupling reaction catalyzed by palladium nanocubes. *ACS Catal.* **2017**, *7*, 1462−1469.
(18) NIST X-ray Photoelectron Spectroscopy Database, *NIST Standard Reference Database Number 20*; National Institute of Standards and Technology: Gaithersburg, MD, 2000.
(19) Cai, Y.; Long, X.; Luo, Y.-H.; Zhou, C.; Rittmann, B. E. Stable dechlorination of Trichloroacetic Acid (TCAA) to acetic acid catalyzed by palladium nanoparticles deposited on H2-transfer membranes. *Water Res.* **2021**, *192*, No. 116841.
(20) Long, M.; Long, X.; Zheng, C.-W.; Luo, Y.-H.; Zhou, C.; Rittmann, B. E. Para-chlorophenol (4-CP) removal by a palladium-coated biofilm: coupling catalytic dechlorination and microbial mineralization via denitrification. *Environ. Sci. Technol.* **2021**, *55*, 6309−6319.
(21) Freitas, A.; Mendes, M.; Coelho, G. Thermodynamic study of fatty acids adsorption on different adsorbents. *J. Chem. Thermodyn.* **2007**, *39*, 1027−1037.
(22) Lefèvre, G.; Preočanin, T.; Lützenkirchen, J. Attenuated total reflection-infrared spectroscopy applied to the study of mineral-aqueous electrolyte solution interfaces: a general overview and a case study. In *Infrared Spectroscopy-Materials Science, Engineering and Technology*; IntechOpen: 2012; vol. *1*, pp. 97−122.
(23) Zalineeva, A.; Baranton, S.; Coutanceau, C. How do Bi-modified palladium nanoparticles work towards glycerol electro-oxidation? An in situ FTIR study. *Electrochim. Acta* **2015**, *176*, 705−717.
(24) Gao, X.; Chorover, J. Adsorption of perfluorooctanoic acid and perfluorooctanesulfonic acid to iron oxide surfaces as studied by flow-through ATR-FTIR spectroscopy. *J. Environ. Chem.* **2012**, *9*, 148−157.
(25) Saldan, I.; Semenyuk, Y.; Marchuk, I.; Reshetnyak, O. Chemical synthesis and application of palladium nanoparticles. *J. Mater. Sci.* **2015**, *50*, 2337−2354.
(26) Teschner, D.; Borsodi, J.; Wootsch, A.; Révay, Z.; Hävecker, M.; Knop-Gericke, A.; Jackson, S. D.; Schlögl, R. The roles of subsurface carbon and hydrogen in palladium-catalyzed alkyne hydrogenation. *Science* **2008**, *320*, 86−89.
(27) Selinsek, M.; Deschner, B. J.; Doronkin, D. E.; Sheppard, T. L.; Grunwaldt, J.-D.; Dittmeyer, R. Revealing the structure and mechanism of palladium during direct synthesis of hydrogen peroxide in continuous flow using operando spectroscopy. *ACS Catal.* **2018**, *8*, 2546−2557.
(28) Luo, S.; Yang, S.; Wang, X.; Sun, C. Reductive degradation of tetrabromobisphenol A over iron−silver bimetallic nanoparticles under ultrasound radiation. *Chemosphere* **2010**, *79*, 672−678.
(29) Chaplin, B. P.; Reinhard, M.; Schneider, W. F.; Schüth, C.; Shapley, J. R.; Strathmann, T. J.; Werth, C. J. Critical review of Pd-based catalytic treatment of priority contaminants in water. *Environ. Sci. Technol.* **2012**, *46*, 3655−3670.
(30) Zhou, C.; Ontiveros-Valencia, A.; Wang, Z.; Maldonado, J.; Zhao, H.-P.; Krajmalnik-Brown, R.; Rittmann, B. E. Palladium recovery in a H2-based membrane biofilm reactor: formation of Pd (0) nanoparticles through enzymatic and autocatalytic reductions. *Environ. Sci. Technol.* **2016**, *50*, 2546−2555.
(31) Wang, Y.; Liu, J.; Wang, P.; Werth, C. J.; Strathmann, T. J. Palladium nanoparticles encapsulated in core−shell silica: A structured hydrogenation catalyst with enhanced activity for reduction of oxyanion water pollutants. *ACS Catal.* **2014**, *4*, 3551−3559.
(32) Zhang, P.; Jiang, F.; Chen, H. Enhanced catalytic hydrogenation of aqueous bromate over Pd/mesoporous carbon nitride. *Chem. Eng. J.* **2013**, *234*, 195−202.
(33) Chen, H.; Xu, Z.; Wan, H.; Zheng, J.; Yin, D.; Zheng, S. Aqueous bromate reduction by catalytic hydrogenation over Pd/Al2O3 catalysts. *Appl. Catal., B* **2010**, *96*, 307−313.
(34) Kopinke, F.-D.; Mackenzie, K.; Koehler, R.; Georgi, A. Alternative sources of hydrogen for hydrodechlorination of chlorinated organic compounds in water on Pd catalysts. *Appl. Catal., A* **2004**, *271*, 119−128.
(35) Xiao, F.; Simcik, M. F.; Halbach, T. R.; Gulliver, J. S. Perfluorooctane sulfonate (PFOS) and perfluorooctanoate (PFOA) in soils and groundwater of a US metropolitan area: Migration and implications for human exposure. *Water Res.* **2015**, *72*, 64−74.
(36) Yong, Z. Y.; Kim, K. Y.; Oh, J.-E. The occurrence and distributions of per-and polyfluoroalkyl substances (PFAS) in groundwater after a PFAS leakage incident in 2018. *Environ. Pollut.* **2021**, *268*, No. 115395.
(37) Greco, R.; Goessler, W.; Cantillo, D.; Kappe, C. O. Benchmarking immobilized di-and triarylphosphine palladium catalysts for continuous-flow cross-coupling reactions: efficiency, durability, and metal leaching studies. *ACS Catal.* **2015**, *5*, 1303−1312.

https://doi.org/10.1021/acs.est.1c06528
Environ. Sci. Technol. 2021, 55, 16699−16707

(38) Cantillo, D.; Kappe, C. O. Immobilized Transition Metals as Catalysts for Cross-Couplings in Continuous Flow—A Critical Assessment of the Reaction Mechanism and Metal Leaching. *ChemCatChem* **2014**, *6*, 3286−3305.

https://doi.org/10.1021/acs.est.1c06528
Environ. Sci. Technol. 2021, 55, 16699−16707